J Solid State Electrochem (2010) 14:555–563
DOI 10.1007/s10008-008-0747-4

ORIGINAL PAPER

Impedance study of adsorption of iodide ions at Cd(0001) and Bi(111) electrode from various solutions with constant ionic strength

L. Siinor · V. Ivaništšev · K. Lust · E. Lust

Received: 30 June 2008 / Revised: 18 November 2008 / Accepted: 18 November 2008 / Published online: 13 December 2008

Abstract Adsorption of iodide ions at the Bi(111) and Cd (0001) electrodes from the aqueous solutions with constant ionic strength $0.1x$ M KI+$0.1(1-x)$ M KF and $0.1x$ M KI+ $0.033(1-x)$ M K_2SO_4 has been studied by impedance spectroscopy. It was found that, to a first approximation, the classical Frumkin–Melik–Gaikazyan equivalent circuit with the slow diffusion-like and adsorption steps can be applied for fitting the experimental impedance data for iodide ions adsorption on Bi(111) and Cd(0001) from aqueous solutions with constant ionic strength. The modified Grafov–Damaskin circuit can be used in the region of electrode potentials, where parallel faradic processes (electroreduction of protons, oxygen traces) are probable. The more complicated Ershler equivalent circuit, taking into account the slow diffusion-like, adsorption and charge transfer steps, is not applicable for characterization of the adsorption process of I^- at Bi(111) and Cd(0001) electrodes.

Keywords Impedance spectroscopy · Adsorption kinetics · Halide ions · Bi single crystal · Cd single crystal

Introduction

Although the adsorption of halide ions from aqueous and non-aqueous solutions on the single crystal planes of various metals has been investigated by several electrochemists [1–21], there are only few works devoted to the adsorption kinetics of halide and other anions on various single crystal plane electrodes—Au (*hkl*), Ag (*hkl*), Pt (*hkl*), and Rh (111)—from aqueous solutions and on Bi (*hkl*) from non-aqueous solutions [1, 5, 6]. The adsorption of halide ions as well as other anions seems to be a kinetically complicated process [1–33] and the structure of the adsorption layer depends on the electrode potential E, chemical composition, and concentration of adsorbing ions as well as on the chemical composition of metal and solvent studied [5, 6, 31]. The capacitance dependence on ac frequency has been explained by low adsorption rate of specifically adsorbed anions (Cl^-, Br^-, and I^-) on Au (*hkl*) [1, 8]. For Ag(111) electrode, adsorption of the Cl^- ions starts near −0.7 V (vs. saturated calomel electrode, SCE) while adsorption of the Br^- ions starts at $E=-1.0$ V (SCE) [8], which is explained by the competitive adsorption of halide ions and solvent molecules. Ex situ reflection energy electron diffraction and in situ STM investigations show a disordered adlayer up to potential of −0.1 V and an ordered adlayer for the anions as an unrotated (1.38×1.38) structure and $\left(\sqrt{3}\times\sqrt{3}\right)$ R 30^0 adlayer for Br^- ions [10–17]. At electrode potentials more positive than the potential of sharp capacitance (C) peak in the C, E curves or the current density peak in the current density j vs. E curves, the more compressed overlayer structure has been observed [16, 17]. However, the sum of the ideal double layer capacitance C_{dl} and low-frequency adsorption capacitance C_{ad} as a total low-frequency thermodynamic series capacitance C_0, independent of ac frequency, could be obtained only at low frequency (f<2 Hz) and for real surfaces the situation is even more complicated [2].

Thermodynamics of the halides adsorption has been analyzed [18–21, 24–30] and there are differences in the

Contribution to the Fifth Baltic Conference on Electrochemistry, 30 April–3 May 2008, Tartu, Estonia

L. Siinor · V. Ivaništšev · K. Lust · E. Lust (✉)
Institute of physical Chemistry, Tartu University,
2 Jakobi str.,
51013 Tartu, Estonia
e-mail: enn.lust@ut.ee

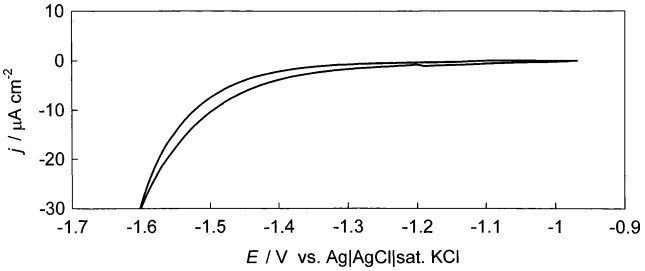

Fig. 1 Cyclic voltammetry curves for Cd(0001) electrode in K_2SO_4 at scan rate 10 mV s^{-1}

thermodynamic data obtained using various measurement methods, mainly caused by the slow adsorption rate of the halide anions. For example, Shi et al. [19] observed that the charge densities calculated by using differential capacitance, chronocoulometry, and voltammetry methods differ noticeably even if the same surface preparation method of a single crystal electrode has been used.

This work is focused on the impedance study [34–42] of adsorption of iodide ions on the surface of the electrochemically polished Bi(111) and Cd(0001) electrodes. The purpose of the present work is to obtain the impedance parameters and limiting stages for iodide ions adsorption from aqueous solutions with constant ionic strength based on various surface inactive electrolyte solutions. It should be noted that the adsorption kinetics of ions is important because the I^-, Br^-, Cl^-, HSO_4^-, $H_2PO_4^-$ etc. anions have a big influence on the kinetics of hydrogen evolution and corrosion of various metals and technologically important alloys [43–46]. The electrochemical kinetics of various reactions (electroreduction of anions, cations, and organic compounds) and electro-synthesis/electro-analysis conditions are noticeably influenced by chemical composition of the surface inactive electrolyte [23, 28, 31].

Experimental

The adsorption kinetics of iodide ions at electrochemically polished Bi(111) and Cd(0001) single crystal planes [31, 43–46] from aqueous solutions with constant ionic strength $0.1x$ M KI+$0.1(1-x)$ M KF and $0.1x$ M KI+$0.033(1-x)$ M K_2SO_4 was studied by means of impedance spectroscopy (x is a mole fraction of KI in solution) [5, 6, 18–21] and cyclic voltammetry. The systems with constant ionic strength were selected to minimize the influence of the changes in the diffuse layer structure. The solutions were prepared from KF, K_2SO_4, and KI (Aldrich Chemical Company, 99.998%) and Milli Q+ water. The quality of the Bi single crystal electrode was tested by X-ray diffraction, in situ STM, AFM, and ultra high vacuum STM methods [22, 23]. Before each experiment, a disk-like Bi(111) electrode (surface area 0.1 cm^2) was electrochemically polished in an aqueous KI+HCl solution and Cd(0001) in aqueous H_3PO_4 solution [5, 6, 23, 31–33]. After polishing the electrode was carefully rinsed with ultra purified water, submerged into the surface inactive electrolyte solution (previously saturated with hydrogen) under potential control at −1.2 V (vs. Ag | AgCl | sat. KCl here and below, connected to the main part of the cell through a long Luggin capillary) and polarized for nearly 2 h at E=−1.2 V. The impedance spectra were measured at f from 0.1 to 1×10^4 Hz (75 different frequencies) in the potential region from −1.6 V to −0.5 V and −1.4 to −0.975 V in the case of Bi(111) and Cd(0001), respectively, using the Autolab PGSTAT 30 FRA 2 measurement system. No considerable surface changes occur on the Bi and Cd single crystal electrodes in the corresponding potential ranges [5, 6, 22, 23, 31–33, 43–46].

Results and discussion

The cyclic voltammetry (j vs. E) curves show that the Bi (111) and Cd(0001) electrodes are nearly ideally polarizable within the regions of $-1.4<E$ −0.55 V and $-1.35<E$ −0.95 V, respectively (Fig. 1).

The impedance complex plane (Z'',Z')—plots for Bi(111) and Cd(0001) electrodes at different electrode potentials and mole fractions of KI are shown in Figs. 2 and 3 (Z' is a

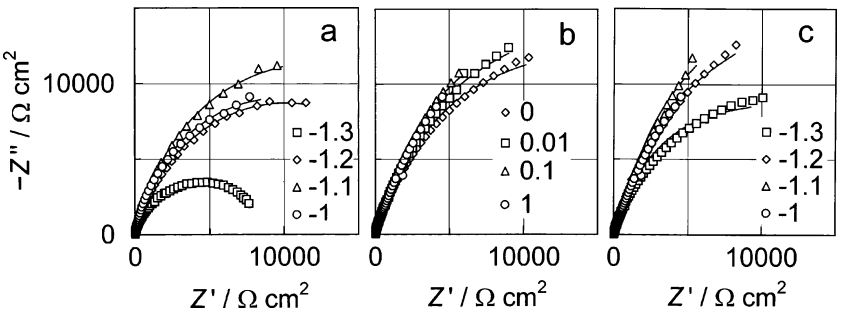

Fig. 2 Impedance complex plane plots for Cd(0001) in $0.1x$ M KI+$0.033(1-x)$ M K_2SO_4 (**a**) and in $0.1x$ M KI+$0.1(1-x)$ M KF (**b**, **c**) at the mole fraction of KI: x=0.5 (**a**) and x=1.0 (**c**) at various electrode potentials (noted in figure), and at −1.0 V (**b**) for various x (noted in figure) *Marks* experimental data and *solid lines* fitting according to the Frumkin–Melik–Gaikazyan equivalent circuit (EC A in Fig. 6a)

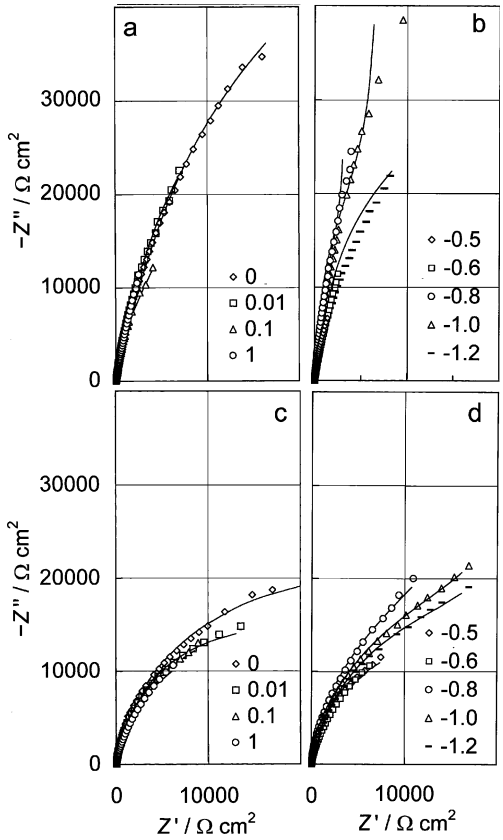

Fig. 3 Impedance complex plane plots for the Bi(111) in 0.1*x* M KI+ 0.033(1–*x*) M K_2SO_4 (**a**, **b**) and in 0.1*x* M KI+0.1(1–*x*) M KF (**c**, **d**) at the electrode potential –0.6 V and mole fractions of KI, *x*, noted in figure (**a**, **c**), and at *x*=1.0 (**b**) and *x*=0.5 (**d**) at various electrode potentials (Vvs.Ag|AgCl|sat.KCl), noted in figure. *Marks* experimental data and *solid lines* fitting according to equivalent EC B (Fig. 6a) (**b**, **c**, **d**) and EC A (**a**)

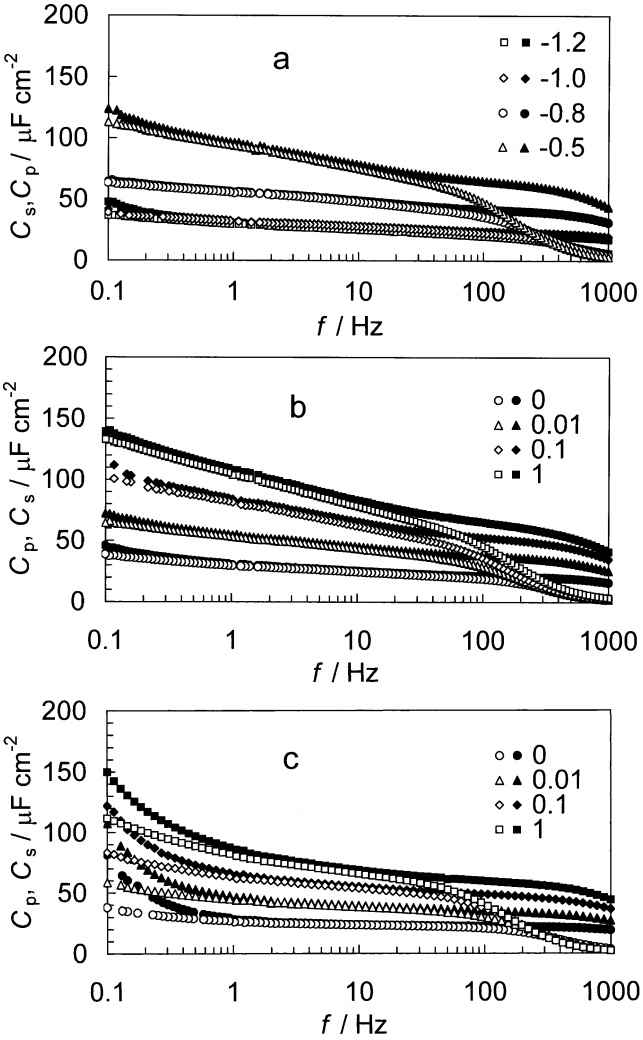

Fig. 5 Dependence of series capacitance C_s (*filled marks*) and parallel capacitance (*open marks*) on frequency for Bi(111) in 0.1 M KI at various electrode potentials (noted in figure) (**a**), and for 0.1*x* M KI+ 0.033(1–*x*) M K_2SO_4 solutions (**b**) and in 0.1*x* M KI+0.1(1–*x*) M KF solutions (**c**) at –0.6 V for various mole fractions of KI, noted in figure

real part of the impedance and *Z″* is an imaginary component of impedance equal to $(jC_s\omega)^{-1}$, where $j=\sqrt{-1}$ is the imaginary unit, C_s is the total series capacitance at fixed angular frequency $\omega=2\pi f$, where *f* is ac frequency

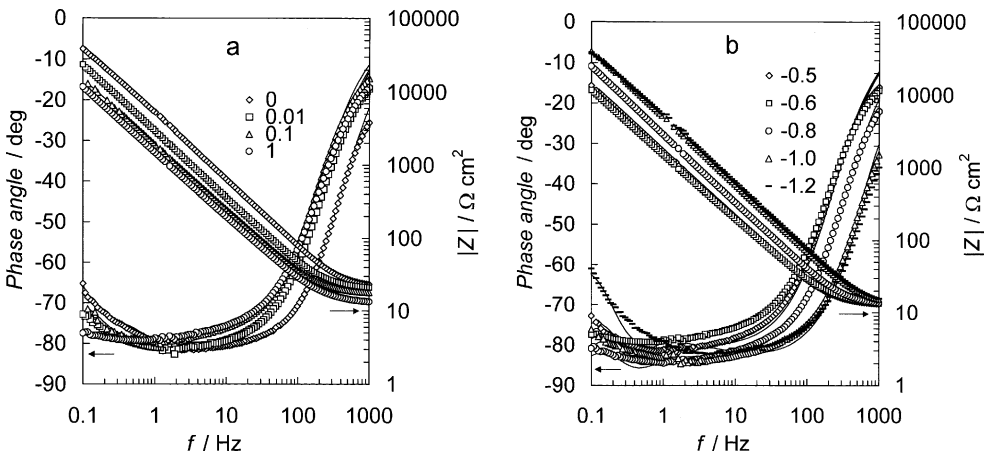

Fig. 4 Bode phase angle and impedance modulus vs. frequency plots for Bi(111) in 0.1*x* M KI+ 0.033(1–*x*) M K_2SO_4 solution at the electrode potential –0.6 V and mole fractions of KI, *x*: noted in figure (**a**), and at *x*=1.0 and various electrode potentials (Vvs.Ag|AgCl|4MKCl), noted in figure (**b**). *Marks* experimental data and *solid lines* fitting according to EC A (Fig. 6a)

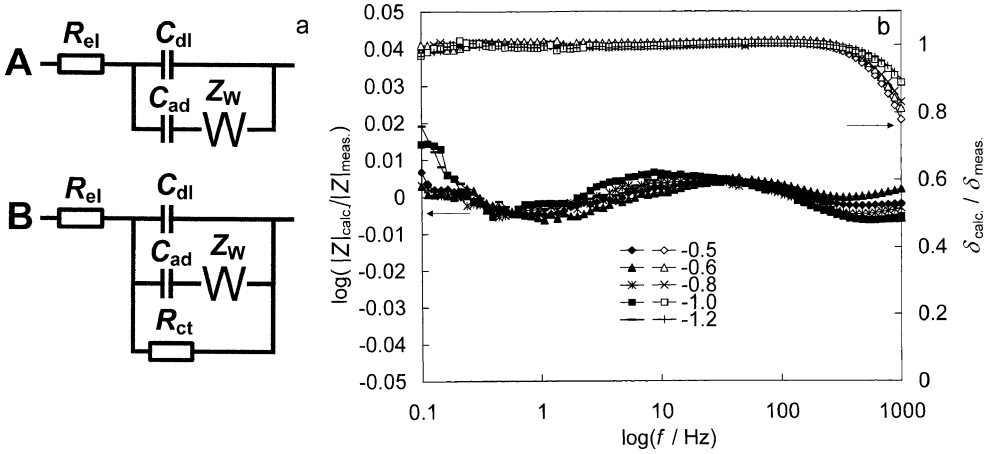

Fig. 6 **a** Frumkin–Melik–Gaikazyan equivalent circuit (*A*) and modified Grafov–Damaskin equivalent circuit (*B*), where R_{el} is the electrolyte resistance, C_{dl} is the double layer capacitance, C_{ad} is adsorption capacitance, R_D is diffusion resistance, and R_{ct} is charge transfer resistance. **b** $\log\left(|Z|_{calculated}/\log|Z|_{measured}\right)$ vs. log*f* plots (*filled marks*) and $\delta_{calculated}/\delta_{measured}$ vs. log*f* plots (*open marks*) for Bi (111) electrode in 0.1 M KI solution at various potentials (V vs. Ag|AgCl|sat. KCl, noted in figure) in the case of circuit B

[34–40]). The shape of the Z″,Z′ plots depends noticeably on the electrode potential and on the amount of the surface active electrolyte KI in the solution. The shape of the Z″,Z′ plots depends also on the chemical composition of the surface inactive electrolyte (Figs. 2 and 3). For KF+KI | Bi (111) or Cd(0001) systems the more pronounced mixed kinetic behavior can be seen (see analysis below), caused by competitive adsorption of F^- and I^- ions at Bi(111) as

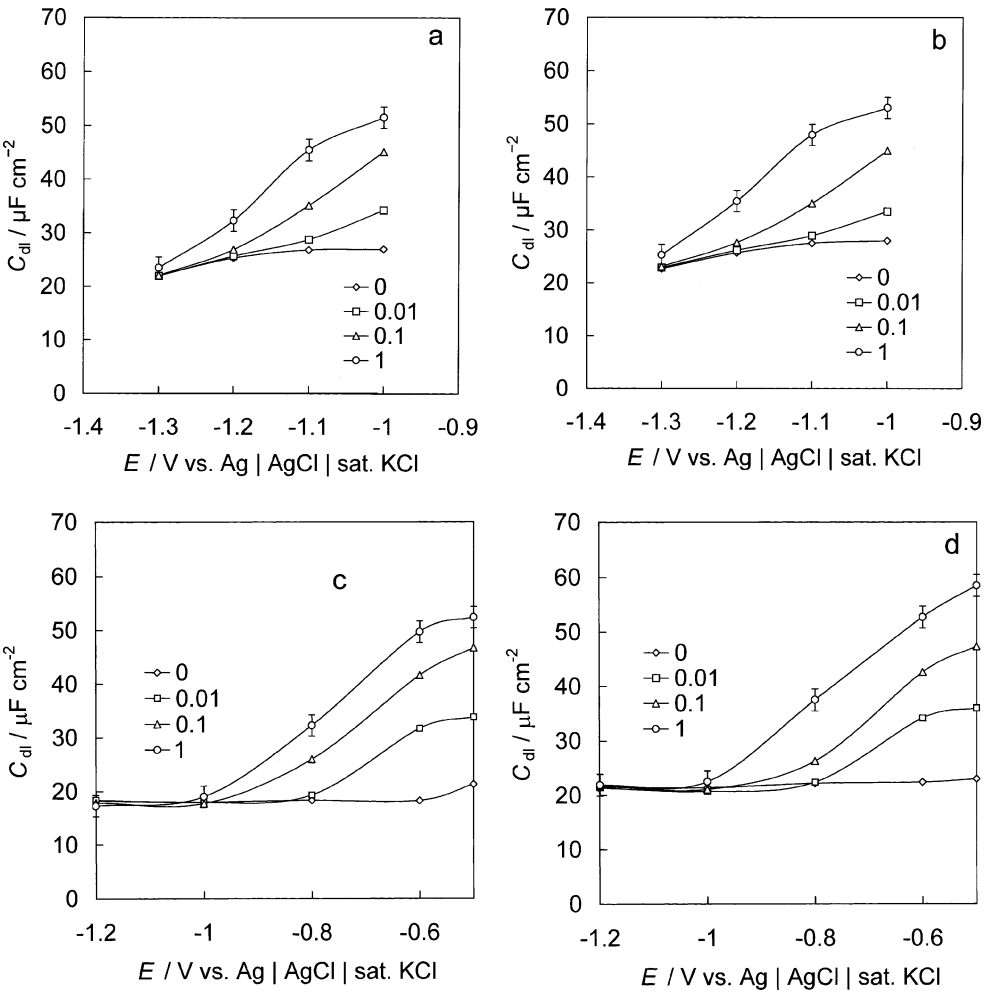

Fig. 7 Dependences of double layer capacitance C_{dl} (calculated according to EC (B) in Fig. 6) on electrode potential for Cd (0001) electrode (**a**, **b**) and Bi (111) electrode (**c**, **d**) in 0.1*x* M KI+0.033(1–*x*) M K_2SO_4 (**a**, **c**) and in 0.1*x* M KI+0.1(1–*x*) M KF (**b**, **d**) at various mole fractions of KI, *x*, noted in figure

well as at Cd(0001) planes. In the region of intensive increase of the differential capacitance C_s ($-0.7<E\leq-0.5$ V for Bi(111) and $-1.1<E<-0.975$ V for Cd(0001)) the impedance spectra have a complicated shape and can be fitted by tilted non-linear curves, characteristic mainly of the adsorption limited stage, rather than by the semicircles, characteristic of the true faradic process [34–40, 43–46].

The deviation of Bi(111) and Cd(0001) planes from the ideally capacitive behavior (the value of phase angle $\delta = \arctan(Z''/Z')$ is equal to −90°) is visible in the δ vs. log$f$ plots. The value of δ for Cd(0001) at low frequency is less negative (−45° at −1.2 V) than that for Bi(111) (−60°) (Fig. 4). It is important to mention that the deviation of Cd (0001) and Bi(111) from ideally capacitive electrode (adsorption step limitation) in KF+KI electrolyte system decreases with increasing the molar fraction of KI.

The log(−Z″), log$f$ plots for Cd(0001) and Bi(111) in K_2SO_4+KI (not shown for shortness) are linear at f>1 Hz and the values of (–Z″) decrease somewhat with the increase of mole fraction of KI and decrease of negative electrode potential. This effect can be explained by adsorption of I^- anions at Bi(111) and Cd(0001) electrodes, which is very well visible in Fig. 5, where the series capacitance C_s vs. log$f$ plots and parallel capacitance C_p vs. log$f$ plots are compared (C_p has been calculated from C_s according to the mathematical presumption of the complex impedance data as series and parallel RC-circuits [34–38]). The C_s and C_p vs. log$f$ dependences are linear and coincide within the region from 0.5 to 100 Hz. At f<0.5 Hz the noticeable increase in C_s for Cd(0001) | KF+KI contrary to Bi(111)| KF+KI system can be explained by less ideal behavior of Cd(0001) in KF+KI solution. The deviation from linearity is less pronounced in K_2SO_4+KI solutions.

Experimental impedance data were fitted by using the equivalent circuits (Fig. 6a), where R_{el} is the high-frequency series resistance equal to the electrolyte solution resistance R_{el} at $f \to \infty$; C_{dl} is the so-called ideal high-frequency differential double layer capacitance obtained at $f \to \infty (C_{dl} = (\partial q/\partial E)_{\Gamma,\mu}$, where q is electrode charge density, Γ is Gibbs adsorption of anions adsorbed and μ is chemical potential of surface active compound); adsorption capacitance C_{ad} is equal to $(C_0 - C_{dl}) = (\partial q/\partial\Gamma)_E (\partial\Gamma/\partial E)_\mu$, where thermodynamic low-frequency capacitance $C_0 = (\partial q/\partial E)_{\Gamma,\mu} + (\partial q/\partial\Gamma)_E (\partial\Gamma/\partial E)_\mu$ is

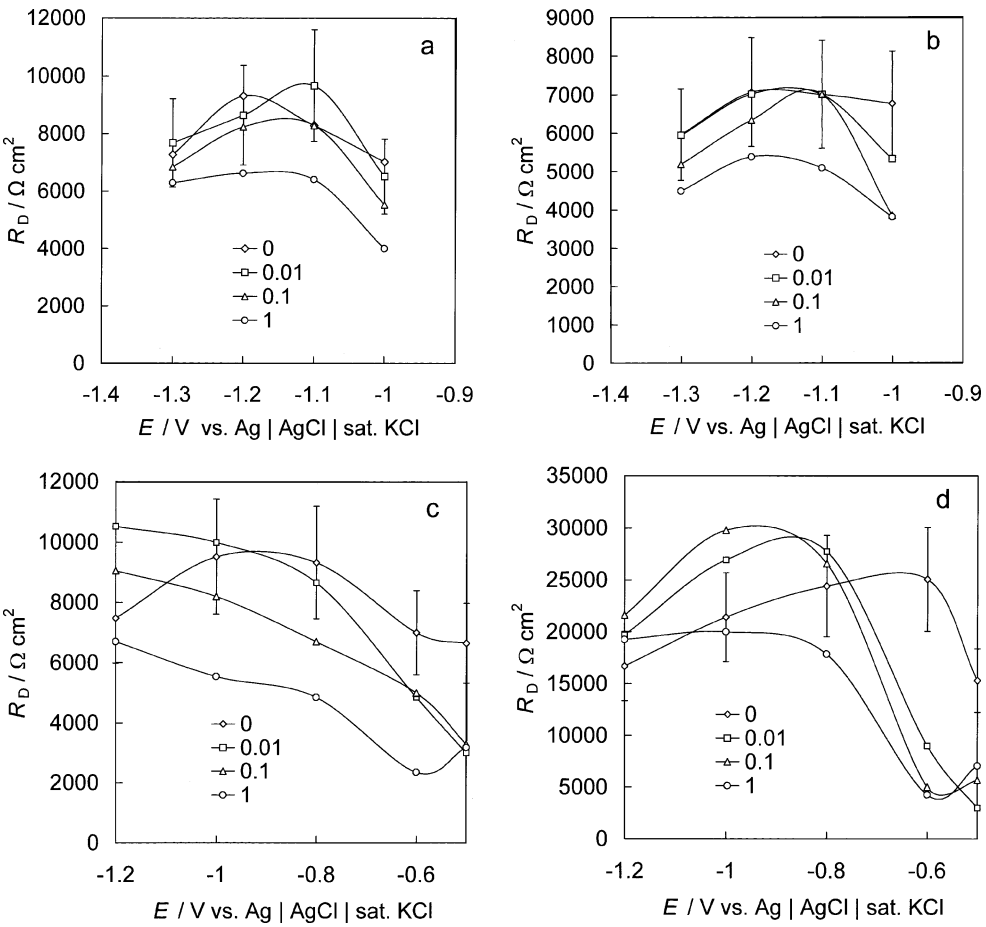

Fig. 8 Dependences of diffusion resistance R_D (calculated according to EC (B) in Fig. 6) on electrode potential for Cd (0001) electrode (**a**, **b**) and Bi (111) electrode (**c**, **d**) in 0.1x M KI+0.033(1–x) M K_2SO_4 (**a**, **c**) and in 0.1x M KI+0.1(1–x) M KF (**b**, **d**) at various mole fractions of KI, x, noted in figure

obtained at $f \rightarrow 0; Z_w = \sigma_{ad}(j\omega)^{-1/2}$ is Warburg-like diffusion impedance $\sigma_{ad} = \tau_D^{1/2} C_{ad}^{-1}$ is Warburg-like constant where τ_D is diffusion relaxation time); R_{ct} is the resistance of the very slow parallel charge transfer or true faradic process (probably the hydrogen evolution) [31, 34–37, 45, 46]. A program Zview 2.2 [39] was used for fitting the Z″, Z′-plots (solid lines in Figs. 2 and 3) and other experimental data. The goodness of the fits for all experimental data measured was estimated by the value of the χ^2 function (always smaller than 0.002), weighted sum of squares (Δ^2) and by the relative errors of each parameter in the equivalent circuit (EC) (discussed later in text), keeping the number of data points constant. In addition, the $\log|Z|_{calculated}/\log|Z|_{measured}$ and $\delta_{calculated}/\delta_{measured}$ vs. log$f$ plots have been calculated and analyzed. According to the data in Fig. 6b, the low differences in $|Z|_{calculated}$ and $|Z|_{measured}$ as well as $\delta_{calculated}$ and $\delta_{measured}$ have been obtained, indicating that a good fit of experimental and calculated data has been achieved.

To a first approximation, a good fit of impedance data was obtained with the Frumkin–Melik–Gaikazyan equivalent circuit (FMG) (EC A in Fig. 6a) [31, 34, 41, 42]. The impedance and capacitance functions have the following forms for FMG [34],

$$Z(\omega) = R_{el} + \left\{ j\omega C_{dl} + \left[\left(\sigma_{ad} \Big/ \sqrt{j\omega} \right) + (1/j\omega C_{ad}) \right]^{-1} \right\}^{-1} \quad (1)$$

$$C(\omega) = \{ j\omega [Z(\omega) - R_{el}] \}^{-1} = C_{dl} + C_{ad} \Big/ \left(1 + \sigma_{ad} C_{ad} \sqrt{j\omega} \right) \quad (2)$$

Similarly to Bi(001) | KF+KI interface [31], inserting the adsorption resistance R_{ad} into FMG (i.e. building up the Ershler circuit [35] (or more widely known as the Randles–Frumkin–Melik–Gaikazyan model [36–38]), where R_{ad} is added in series with adsorption capacitance and Warburg-like diffusion impedance), taking into account the resistance of slow specific adsorption step, did not afford considerable decrease of the χ^2-function and Δ^2 values. Moreover, the values of R_{ad} are very low (~0.1 Ω cm^2) with very high error values (~5,000%).

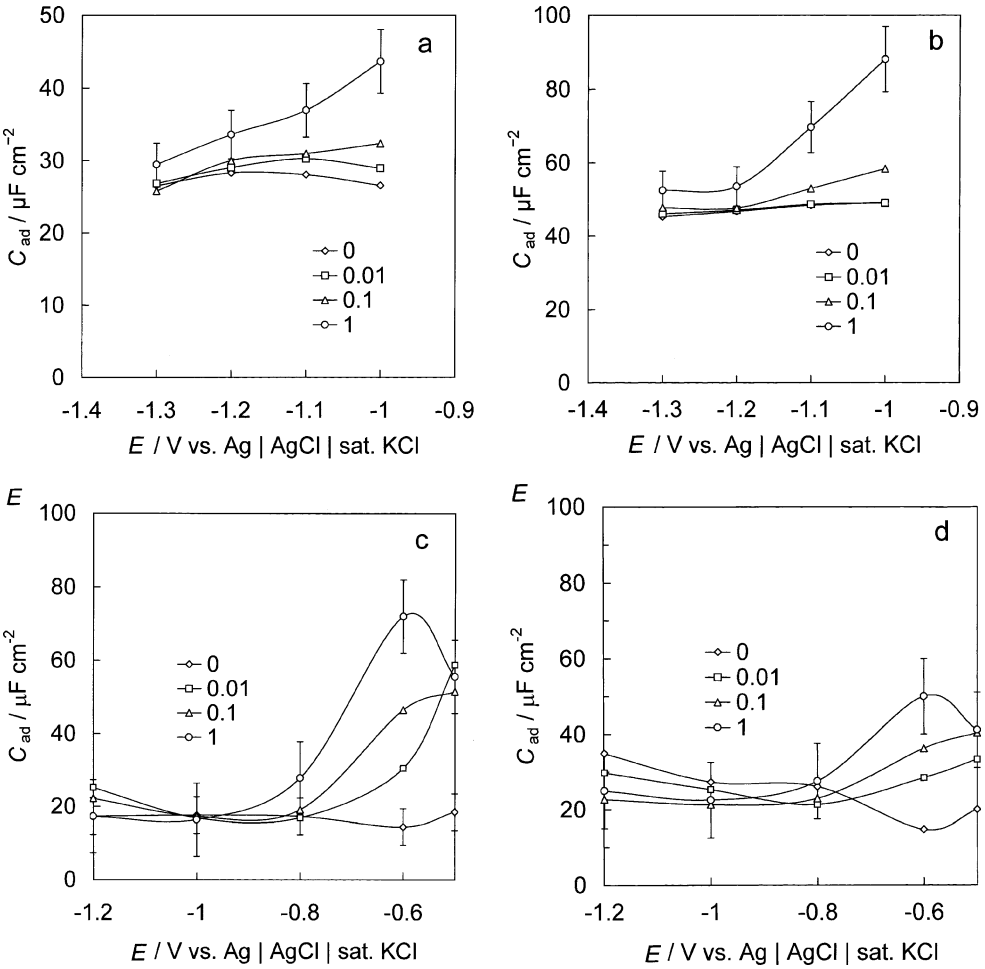

Fig. 9 Dependences of adsorption capacitance C_{ad} (calculated according to EC (B) in Fig. 6) on electrode potential for Cd (0001) electrode (**a**, **b**) and Bi (111) electrode (**c**, **d**) in 0.1x M KI+0.033(1–x) M K_2SO_4 (**a**, **c**) and in 0.1x M KI+0.1(1–x) M KF (**b**, **d**) at various mole fractions of KI, x, noted in figure

Somewhat better fit (30…40% lower χ^2-function values, i.e. better overlapping of calculated impedance data with experimental ones) was established if the modified Grafov–Damaskin (MGD) model had been applied (EC B in Fig. 6a). The applicability of FMG and MGD depends on the electrode potential applied. FMG does not give quite good fitting if the slow parallel faradic reactions occur on Cd(0001) at $E<-1.4$ V or on Bi(111) at $E<-1.2$ V, respectively (Figs. 2–4). However, MGD gives a good fit within the whole potential range studied and therefore the parameters obtained using EC (B) will be analyzed in more detail. Also the experimental error bars, obtained using the data of more than five independent experiments and corresponding fits (solid lines), have been given in figures.

According to fitting data, the electrolyte resistance R_{el} (fitting error ≈1%) is independent of electrode potential, but there is a weak dependence of R_{el} on the concentration of the surface active component (KI) because the molar conductivity of KI is somewhat higher than that for KF or K_2SO_4 and the resistance of the electrolyte solution decreases with increasing c_{KI}.

The so-called ideal double layer capacitance C_{dl}, (Fig. 7, fitting error ~1%) obtained at $f \to \infty$ by fitting of the impedance spectra, changes in the same way as the series (so called total differential) capacitance measured at fixed low frequency by using the traditional differential capacitance method [31–33], i.e. a relatively steep rise occurs as the electrode potential becomes less negative than −1.1 V for Cd(0001) and −0.7 V for Bi(111) (Fig. 7). The dependence of C_{dl} on the mole fraction of KI can be explained with the specific adsorption of I^- on the Bi(111) and also Cd(0001) surfaces at less negative electrode potentials [23, 31–33]. Hence, the inner layer structure depends on the values of Gibbs adsorption Γ of the I^- ions. C_{dl} for mixed electrolyte solutions is weakly higher in KI+KF compared with KI+K_2SO_4 system for Bi(111).

The Warburg-like diffusion impedance, to a first approximation, can be simulated by the generalized finite Warburg element for a short circuit terminus model [31,37,45–48], expressed as:

$$Z_w = R_D \tanh[(jT\omega)^{\alpha_w}]/(jT\omega)^{\alpha_w} \quad (3)$$

where R_D is the limiting diffusion resistance; the so called mass transfer frequency parameter T is equal to L^2/D, where L is the effective diffuse layer thickness and D is the effective diffusion coefficient of the particles; α_W is the diffusion impedance fractional exponent varying from 0 to 1. The results of fitting show that the values of α_W deviate

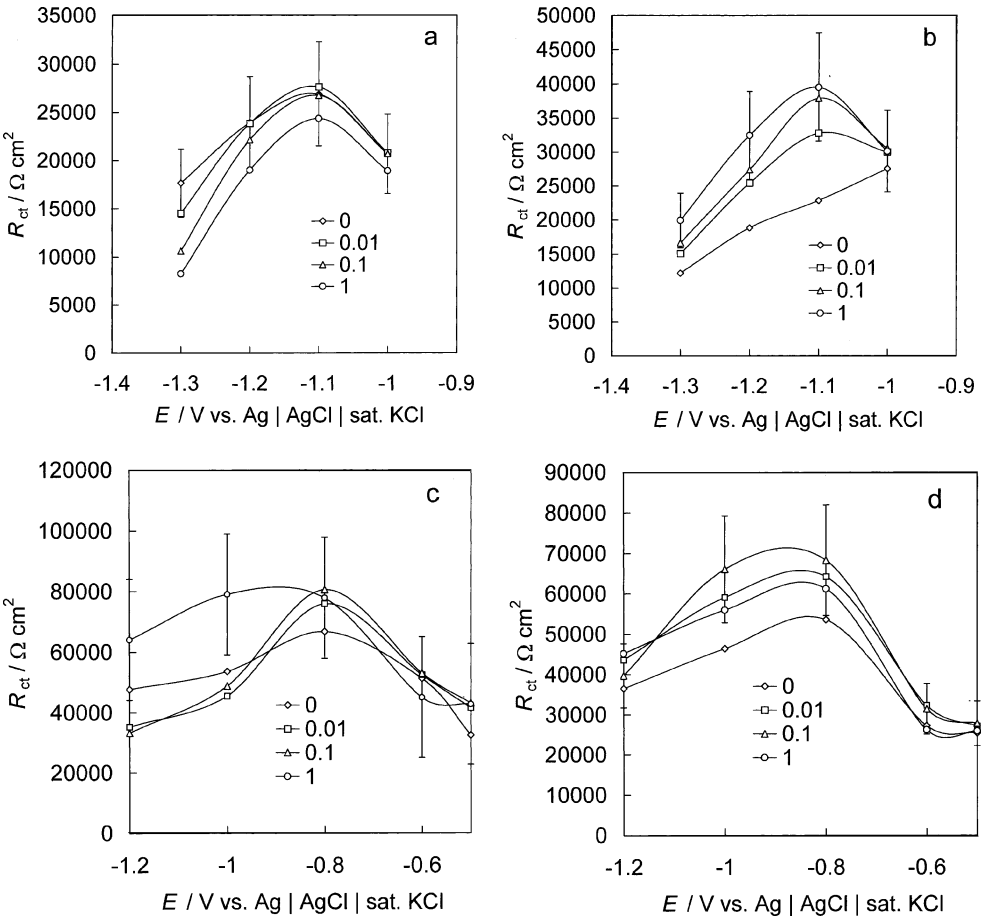

Fig. 10 Dependences of charge transfer resistance R_{ct} (calculated according to EC (B) in Fig. 6) on electrode potential for Cd(0001) electrode (**a**, **b**) and Bi(111) electrode (**c**, **d**) in 0.1x M KI+0.033(1–x) M K_2SO_4 (**a**, **c**) and in 0.1x M KI+ 0.1(1–x) M KF (**b**, **d**) at various mole fractions of KI, x, noted in figure

from 0.5 (with an experimental error ±0.15 and fitting error 2%), demonstrating some deviation of the Cd(0001) and Bi (111) | aqueous solution interface from the semi-infinite diffusion model [34–37, 43,44]. As can be seen in Fig. 8, the computed dependences of diffusion-like resistance R_D (fitting error ~5%) have a maximum at moderate electrode potential (at −0.7 V for Bi(111) and at −1.0 V for Cd (0001)). R_D depends weakly on the surface inactive electrolyte composition and electrode material, and decreases with growing mole fraction of KI. The same effect has been established for Bi(hkl) | non-aqueous surface active electrolyte systems (LiI), and the decrease in R_D at less negative potentials can be explained by adsorption of the I^- ions at the electrode surface [5, 6, 31–33]. In addition, it should be noted that the calculated values of the diffusion coefficient are very high, which could be caused by deviation of our system from the classical semi-infinite diffusion model toward the generalized finite-length Warburg element for short circuit terminus model [31, 37, 47, 48], explaining the deviation of the fitted α_W from 0.5 for Bi(111) and Cd(0001) | KI+KF or KI+K_2SO_4 aqueous solution interfaces.

The value of adsorption capacitance C_{ad} (Fig. 9, fitting error ~5%) increases with mole fraction of KI in the region of potentials where specific adsorption of I^- ions occurs. It should be noted that EC (B) (Fig. 6a) has to be used to receive the reasonable values of C_{ad}, i.e. a slow faradic process has to be taken into account [31, 41, 42]. The increase in the values of C_{ad} with increasing c_{KI} has been observed, which can be explained by the intensive specific adsorption of iodide ions at the electrodes [24–30].

Charge transfer resistance R_{ct} (Fig. 10, fitting error ~7%) is maximal at E=−1.1 V for Cd(0001) and at E=−0.9 V for Bi(111), indicating the occurrence of slow electroreduction process (hydrogen evolution, reduction of oxygen traces etc.) at E<−1.2 V for both electrodes, in agreement with cyclic voltammetry data.

As mentioned before, differently from Au(111) | halide system [1] the Ershler model [35] (or Randles–Frumkin–Melik–Gaikazyan model as it is more widely called in modern literature [31, 36–38, 41, 42]) is not applicable for Bi(111) or Cd(0001) | halide aqueous solution interface because the values of the adsorption resistance are very small (≈0) and the fitting errors are very high (over 5,000%). Therefore, the nearly reversible adsorption of the halide ions at −1.2<E<−0.5 V for Bi(111) and −1.2<E<−0.975 V for Cd(0001) has been assumed to occur.

Conclusions

Impedance spectroscopy method applied for studying of the I^- ions adsorption kinetics at Bi(111) and Cd(0001) electrode in aqueous solutions with constant ionic strength shows that the reproducible data in aqueous solution can be obtained in the range of ac frequencies from 0.1 to 10,000 Hz. The Bi(111) electrode is nearly ideally capacitive within the potential region from −1.2 V to −0.5 V (vs.Ag|AgCl|sat.KCl), and Cd(0001) from −1.2 to −0.975 V in the aqueous solution with constant ionic strength 0.1x M KI+0.1(1−x) M KF or 0.1x M KI+0.033 (1−x) M K_2SO_4. Deviation of Cd(0001) and Bi(111) electrodes from ideally capacitive electrode model is more pronounced in the case of KF containing solutions. Slow hydrogen evolution process [46], electroreduction of oxygen traces and adsorption of K^+ ions is probable on both electrodes at more negative potential than −1.4 V. Experimental impedance data were fitted by using the various equivalent circuits and the good results were obtained with the classical Frumkin–Melik–Gaikazyan model [34]. However, the best fitting of the calculated with experimental impedance data has been established by using the modified Grafov–Damaskin model [41, 42, 45, 46], where the parallel electroreduction process(es) (hydrogen evolution) has been taken into account. The electrical double layer capacitance, adsorption capacitance, diffusion resistance, and other adsorption characteristics depend on the electrode potential applied. However, there is no noticeable dependency of these parameters on the mole fraction of the surface active I^- anion in the electrolyte solution at moderate negative potentials (i.e. in the region where there is no specific adsorption of anions). At E>−1.0 V for Bi (111) and at E>−1.1 V for Cd(0001), there is a noticeable dependence of C_{ad} on the mole fraction of KI, thus, if the intensive specific adsorption of the I^- ions starts. Analysis of complex impedance plane and phase angle vs. ac frequency curves shows that adsorption of I^- anions is limited by mixed kinetics (slow adsorption and diffusion-like steps).

Acknowledgements This work was supported in part by the Estonian Science Foundation under Projects No 5803 and No 6696.

References

1. Pajkossy T, Wandlowski T, Kolb DM (1996) J Electroanal Chem 414:209. doi:10.1016/0022-0728(96)04700-6
2. Jovic VD, Jovic BM (2003) J Electroanal Chem 541:1. doi:10.1016/S0022-0728(02)01309-8
3. Jovic VD, Parsons R, Jovic BM (1992) J Electroanal Chem 339:327. doi:10.1016/0022-0728(92)80461-C
4. Langkau T, Baltruschat H (1998) Electrochim Acta 44:909. doi:10.1016/S0013-4686(98)00194-7
5. Väärtnõu M, Lust E (2002) J Electroanal Chem 533:107. doi:10.1016/S0022-0728(02)01077-X
6. Väärtnõu M, Lust E (2004) J Electroanal Chem 565:211. doi:10.1016/j.jelechem.2003.10.010

7. Eberhardt D, Santos E, Schmickler W (1996) J Electroanal Chem 419:23. doi:10.1016/S0022-0728(96)04872-3
8. Beltramo G, Santos E (2003) J Electroanal Chem 556:127. doi:10.1016/S0022-0728(03)00338-3
9. Frumkin AN (1979) Potentials of zero charge (in Russian). Nauka, Moscow
10. Magnussen O (2002) Chem Rev 102:679. doi:10.1021/cr000069p
11. Jovic BM, Jovic VD, Drazic DM (1995) J Electroanal Chem 399:197. doi:10.1016/0022-0728(95)04291-1
12. Bange K, Straehler B, Sass JK, Parsons R (1987) J Electroanal Chem 229:87. doi:10.1016/0022-0728(87)85132-X
13. Zei MS (1991) J Electroanal Chem 308:295. doi:10.1016/0022-0728(91)85074-Y
14. Aloisi G, Funtikov AM, Will T (1994) J Electroanal Chem 370:297. doi:10.1016/0022-0728(93)03140-K
15. Foresti ML, Aloisi G, Innocenti M, Kobayashi H, Guidelli R (1995) Surf Sci 335:241. doi:10.1016/0039-6028(95)00423-8
16. Koper MTM (1998) J Electroanal Chem 450:189. doi:10.1016/S0022-0728(97)00648-7
17. Mitchell SJ, Brown G, Rikvold PA (2001) Surf Sci 471:125. doi:10.1016/S0039-6028(00)00892-X
18. Parsons R (1955) Trans Faraday Soc 51:1518. doi:10.1039/tf9555101518
19. Shi Z, Wu S, Lipkowski J (1995) J Electroanal Chem 384:171. doi:10.1016/0022-0728(94)03747-Q
20. Shi Z, Lipkowski J (1996) J Electroanal Chem 403:225. doi:10.1016/0022-0728(95)04313-6
21. Schmickler W (1996) Interfacial electrochemistry. Oxford University Press, New York
22. Kallip S, Lust E (2005) Electrochem Commun 7:863. doi:10.1016/j.elecom.2005.06.001
23. Lust E (2002) In: Bard AJ, Stratman M (eds) Encyclopedia of Electrochemistry, vol 1.. Wiley, New York, p 188
24. Damaskin B, Karpov S, Dyatkina S, Palm U, Salve M (1985) J Electroanal Chem 189:183. doi:10.1016/0368-1874(85)80066-6
25. Damaskin B, Pankratova I, Palm U, Anni K, Väärtnou M, Salve M (1987) J Electroanal Chem 234:31. doi:10.1016/0022-0728(87)80160-2
26. Damaskin B, Palm U, Salve M (1987) J Electroanal Chem 218:65. doi:10.1016/0022-0728(87)87006-7
27. Vorotyntsev MA, Golub K (1984) Elektrokhimiya 29:256
28. Vorotyntsev MA (1988) Itogi Nauki i Tekhniki Elektrokhimiya 26:3
29. Schultze JW, Vetter KJ (1973) J Electroanal Chem 44:63. doi:10.1016/S0022-0728(73)80515-7
30. Schmickler W, Guidelli R (1987) J Electroanal Chem 235:387. doi:10.1016/0022-0728(87)85223-3
31. Siinor L, Lust K, Lust E (2007) J Electroanal Chem 601:39. doi:10.1016/j.jelechem.2006.10.031
32. Lust K, Väärtnõu M, Lust E (2002) J Electroanal Chem 532:303. doi:10.1016/S0022-0728(02)00754-4
33. Lust K, Lust E (2003) J Electroanal Chem 552:129. doi:10.1016/S0022-0728(03)00014-7
34. Frumkin AN, Melik-Gaikazyan VI (1951) Dokl Akad Nauk SSSR 77:855
35. Ershler B (1948) Zh Fiz Khim USSR 22:683
36. Sluyters-Rehbach M, Sluyters JH (1970) In: Bard AJ (ed) Electroanalytical Chemistry, vol 4. Marcel Dekker, New York, p 1
37. Lasia A (1999) In: Conway BE, Bockris JOM, White RE (eds) Modern Aspects of Electrochemistry, vol 32. Kluwer/Plenum, New York, p 143
38. Macdonald JR, Johnson WB (1987) In: Macdonald JR (ed) Impedance Spectroscopy. Wiley, New York, p 1
39. ZView for Windows (ver. 22) Scribner, Southern Pines, NC, USA
40. Neves RS, De Robertis E, Motheo AJ (2006) Appl Surf Sci 253:1379. doi:10.1016/j.apsusc.2006.02.010
41. Grafov BM, Damaskin BB (1994) J Electroanal Chem 366:29. doi:10.1016/0022-0728(93)03210-G
42. Stoynov ZB, Grafov BM, Savova-Stoynova ES, Elkin VV (1991) Electrochemical impedance. Nauka, Moscow
43. Nurk G, Jänes A, Lust K, Lust E (2001) J Electroanal Chem 515:17. doi:10.1016/S0022-0728(01)00648-9
44. Jänes A, Lust E (2001) Electrochim Acta 47:967. doi:10.1016/S0013-4686(01)00796-4
45. Thomberg T, Nerut J, Lust E (2006) J Electroanal Chem 586:237. doi:10.1016/j.jelechem.2005.10.001
46. Härk E, Lust K, Jänes A, Lust E (2008) J Solid State Electrochem (accepted, doi:10.1007/s 10008-008-0599-y)
47. Compte A, Metzlek R (1997) J Phys A 30:7277. doi:10.1088/0305-4470/30/21/006
48. Bisquert J, Compte A (2001) J Electroanal Chem 499:112. doi:10.1016/S0022-0728(00)00497-6